1 **Secondary Organic Aerosols from OH Oxidation of Cyclic Volatile Methyl Siloxanes as an Important**

2 **Si Source in the Atmosphere**

3 Chong Han[1,2], Hongxing Yang[1], Kun Li[2,3], Patrick Lee[2], John Liggio[2], Amy Leithead[2], Shao-Meng Li[4]*

4 [1]School of Metallurgy, Northeastern University, Shenyang, 110819, China

5 [2]Air Quality Research Division, Environment and Climate Change Canada, Toronto, Ontario M3H 5T4,

6 Canada

7 [3]Laboratory of Atmospheric Chemistry, Paul Scherrer Institute, Villigen 5232, Switzerland

8 [4]State Key Joint Laboratory of Environmental Simulation and Pollution Control, College of Environmental

9 Sciences and Engineering, Peking University, Beijing, China 100871

10 **Correspondence**: Shao-Meng Li (shaomeng.li@pku.edu.cn)

12 **Short summary:** We presented yields and compositions of Si-containing SOA generated from the reaction

13 of cVMS (D3-D6) with OH radicals. NO_x played negative roles on cVMS SOA formation, while ammonium

14 sulfate seeds enhanced D3-D5 SOA yields at short photochemical ages under high-NO_x conditions. The

15 aerosol mass spectra confirmed that the components of cVMS SOA significantly relied on OH exposure. A

16 global cVMS-derived SOA source strength was estimated to understand SOA formation potentials of cVMS.

18 **Abstract**

19 Cyclic volatile methyl siloxanes (cVMS) are active ingredients in widely used consumer products, which

20 can volatilize into the atmosphere, thus attracting much attention due to their potential environmental risks.

21 While in the atmosphere the cVMS undergo oxidation yielding both gaseous and particulate products. The

22 aerosol yields and compositions from the OH oxidation of four cVMS (D3-D6) were determined under low

23   and high-NO_x conditions in an oxidation flow reactor. The aerosol yields progressively increased from D3

24   to D6, consistent with the volatilities and molecule weights of these cVMS. NO_x can restrict the formation

25   of SOA, leading to lower SOA yields under high-NO_x conditions than under low-NO_x conditions, with a

26   yield decrease between 0.05-0.30 depending on the cVMS. Ammonium sulfate seeds exhibited minor

27   impacts on SOA yields under low-NO_x conditions, but significantly increased the SOA yields in the oxidation

28   of D3-D5 at short photochemical ages under high-NO_x conditions. The mass spectra of the SOA showed a

29   dependence of its chemical compositions on OH exposure. At high exposures, equivalent to photochemical

30   ages of > 4 days in the atmosphere, D4-D6 SOA mainly consisted of C_xH_y and $C_xH_yO_zSi_n$ under low-NO_x

31   conditions, whereas they primarily contained N_mO_z, C_xH_y, $C_xH_yO_1$, $C_xH_yO_{>1}$ and $C_xH_yO_zSi_n$ under high-NO_x

32   conditions. The potential contributions of cVMS to SOA formation in the atmosphere were evaluated using

33   the reported cVMS annual production and the yield data obtained in the present study. A global cVMS-

34   derived (D4-D6) SOA source strength is estimated to be 0.01 Tg yr^{-1}, distributed over major urban centers.

35

36   **1 Introduction**

37   Secondary organic aerosols (SOA), which contribute 50-85% to the mass of atmospheric organic aerosols

38   (OA) (Glasius and Goldstein, 2016), are mainly formed via the partitioning of low volatility products from

39   oxidation of volatile organic compounds (VOCs), semi- and intermediate volatile organic

40   compounds(S/IVOCs) (Riipinen et al., 2012). SOA has attracted significant attention due to their important

41   impacts on climate, ecosystems and human health (Berndt et al., 2016). Global budgets of SOA remain an

42   unresolved issue despite extensive research, largely due to uncertainties associated with aerosol yields and

43   the presence of unconsidered SOA precursors.

44   As one type of anthropogenic VOC and potential SOA precursors, cyclic volatile methyl siloxanes (cVMS)

45   are widely used in industrial applications and personal care products (Genualdi et al., 2011; Krogseth et al.,

46   2013a). cVMS have been classified as high-volume chemicals with an annual production of millions of tons

47   globally (Rücker and Kümmerer, 2015; Ahrens et al., 2014). Studies of cVMS in the environment have

48   focused on investigating health and environmental impacts particularly due to their potential persistence,

49   bioaccumulation and toxicity (Guo et al., 2019; Liu et al., 2018; Farasani and Darbre, 2017; Xu et al., 2019;

50   Kim et al., 2018; Coggon et al., 2018). As a result, the European Council has proposed a restriction on the

51   octamethylcyclotetrasiloxane (D4) and decamethylcyclopentasiloxane (D5) content in wash-off personal

52   care products to a limit of 0.1 mass% by 2020 (Eur-Lex, 2018). The legislative actions notwithstanding,

53   knowledge of environmental behavior of cVMS still needs to be further deepened as compared to their

54   applications and economic significance (Rücker and Kümmerer, 2015).

55   It has been estimated that approximately 90% of cVMS are emitted into the atmosphere due to their high

56   saturation vapor pressures (Allen et al., 1997). Gas-phase cVMS have been observed in both indoor and

57   outdoor air. Tang et al. (2015) reported that cVMS accounted for about one-third of total VOC mass

58   concentration in a classroom. Outdoor air concentrations of cVMS have also been measured at different sites

59   worldwide (Li et al., 2020; Wang et al., 2018; Rauert et al., 2018), increasing from rural to urban sites and

60   consistent with increasing population density (Rücker and Kümmerer, 2015). For example, at a rural site in

61   Sweden, the concentration of hexamethylcyclotrisiloxane (D3), D4, D5 and dodecamethylcyclohexasiloxane

62   (D6) were 0.94, 3.5, 13 and 1 ng/m^3, respectively (Kierkegaard and Mclachlan, 2013), while they were 18,

63   55, 172 and 14 ng/m^3 in urban areas of Toronto in Canada, respectively (Genualdi et al., 2011; Rauert et al.,

64   2018). cVMS have also been detected in the remote Arctic atmosphere, confirming their long-range transport

65   (Genualdi et al., 2011; Krogseth et al., 2013b). Atmospheric half-lives of cVMS are on the order of 30, 15,

66   10 and 6 days for D3-D6, respectively, which allow cVMS to exhibit a hemispherical distribution in the

67   atmosphere (Canada, 2008; Xiao et al., 2015). These lifetimes are driven mostly by reactions with the OH

68   radicals (Xiao et al., 2015; Wang et al., 2013), which generate silanols and dimeric products that can be

69   partitioned to condensed phases (Coggon et al., 2018; Sommerlade, 1993; Wu and Johnston, 2016). Different

70   OH concentrations can partly explain the seasonal variation of cVMS lifetimes that was characterized by

71   longer during winter than in summer (Rücker and Kümmerer, 2015). The loss of cVMS in the atmosphere is

72   negligible through O_3 and NO_3 due to their small reaction rates (Atkinson, 1991). The global loss by the

73   reaction with Cl atoms is less than 5% on account of low Cl concentrations, although it may be higher in

74   some regions where cVMS emissions and Cl sources overlap in both space and time (Alton and Browne,

75   2020). It has been demonstrated that elemental Si is a frequent constituent of nanoparticles in rural and urban

76   areas (Phares et al., 2003; Rhoads, 2003; Bein, 2005; Bzdek et al., 2014) and in remote regions (Li and

77   Winchester, 1990; Li and Winchester, 1993). These Si-containing nanoparticles have previously been

78   attributed to ore smelting processes, but recent studies have shown that Si-containing species are one of the

79   main components in cVMS SOA, suggesting that the oxidation of cVMS may be an important source of Si

80   in atmospheric aerosols (Wu and Johnston, 2016, 2017). In a modeling study, the oxidation products of

81   cVMS (D4, D5 and D6) were considered to quantify the maximum potential for aerosol formation through

82   reactions with the OH radicals (Janechek et al., 2017). Chandramouli and Kamens (2001) demonstrated the

83   gas-particle partitioning of silanols from D5 oxidation by the OH radicals. Wu and Johnston (2016, 2017)

84   analyzed the chemical composition of secondary aerosols from OH oxidation of D4 and D5, showing a large

85   number of monomeric and dimeric products. Janechek et al. (2017, 2019) reported physical properties of

86   SOA generated by OH oxidation of D5, including hygroscopicity, cloud seeding potential and volatility.

87   Charan et al. (2022) measured SOA yields of D5 using chambers and flow tube reactors, emphasizing the

88   importance of the relevant OH concentrations and exposures when extrapolating these laboratory results or

89   comparing with other studies. These studies mainly focused on D5 and occasionally D4 but rarely others. To

90   better understand the SOA-forming potentials of typical cVMS in the atmosphere, accurate yields and

91   molecular compositions of SOA from the oxidation of cVMS under various atmospheric conditions are

92   needed.

93   In this work, the formation of SOA from the oxidation of four cVMS (D3-D6) by OH radicals was

94   investigated in an oxidation flow reactor (OFR). Under various combinations of NO_x and ammonium sulfate

95   seed concentrations, the yields and compositions of SOA formed from the oxidation were measured using a

96   suite of instruments including a scanning mobility particle sizer (SMPS), a proton transfer reaction time of

97   flight mass spectrometer (PTR-ToF-MS) and an aerosol mass spectrometer (AMS). Based on these SOA

98   yields, the contribution of cVMS to SOA in the global atmosphere was estimated using reported cVMS

99   concentrations. The results obtained here can largely improve our understanding of the contribution and

100   composition of SOA from cVMS.

101   **2 Experiments and methods**

102   **2.1 Photo-oxidation experiments**

103   The reactions of cVMS with OH radicals were controlled at a constant temperature (21±1˚C) and relative

104   humidity (35%±2%) in a custom-made oxidation flow reactor (the Environment and Climate Change Canada

105   oxidation flow reactor, ECCC-OFR), which is shown in Fig. S1 of the Supplement and has been described

106   in detail previously (Li et al., 2019a). Briefly, the ECCC-OFR is a fused quartz cylinder (length: 50.8 cm,

107   inner diameter: 20.3 cm) equipped with a conical inlet and 7 outlets. Wall losses of particles and gases in the

108   ECCC-OFR have been shown to be lower than in other OFRs (Huang et al., 2017; Lambe et al., 2011;

109   Simonen et al., 2017; Li et al., 2019a). The length and full angle of cone inlet are 35.6 cm and 30°,

110   respectively, designed to minimize the formation of jetting and recirculation in the OFR. The outlet at the

111 reactor center is a stainless-steel sampling port (inner diameter: 0.18 in) extending 12.7 cm long into the

112 ECCC-OFR. This sampling inlet reduces the impact of potential turbulent eddies caused by the back end of

113 the reactor. The remaining 6 outlets around the perimeter are designed to allow side flows to pass through

114 the OFR as a sheath flow, indirectly reducing wall losses of gases and particles inside the OFR upon sampling.

115 Ozone-free mercury UV lamps for generating OH radicals are housed in small quartz tubes around and in

116 parallel to the quartz reaction cylinder, and a large flow of air through each of these smaller quartz tubes is

117 used to remove the heat produced by the lamps. The relative humidity was adjusted by controlling the ratio

118 of dry air to wet air into the reactor, and was measured using a humidity sensor (Vaisala) at one of the sheath

119 flow outlets (side flows) of the reactor. The volume of the entire ECCC-OFR is about 16 L and the total flow

120 rate is 8 L min^{-1}, leading to a residence time of 2 min in the OFR.

121   OH radicals were produced through the reaction of water vapor with O(^{1}D) formed from O$_3$ photolysis at

122 254 nm. The OH concentration in the ECCC-OFR was regulated by controlling the input voltage and the

123 number of UV lamps. Methanol vapor, introduced into the ECCC-OFR through a bubbler containing

124 methanol solution, was used to determine the OH exposure (i.e., photochemical age, from the multiplication

125 of OH concentration and reaction time) by tracking its decay in the reactor from the reaction with the OH.

126 The decay, or fractional loss, of gas-phase methanol, [MeOH]/[MeOH]$_0$ was measured with the PTR-ToF-

127 MS, and was used to calculate the OH concentration via Equation 1,

$$[OH]=-\frac{1}{k_{MeOH}} \ln \frac{[MeOH]}{[MeOH]_0} \tag{1}$$

129 where k_{MeOH} is the second-order rate constant of methanol reaction with OH at 298 K (9.4×10^{-13} cm^3

130 molecule^{-1} s^{-1}). The OH exposure measurement was offline, because methanol can affect the OH reactivity

131 with cVMS. Under low and high-NO$_x$ conditions described below, the OH exposure varied in the range of

132 5.5×10^{10}-1.8×10^{12} and 8.2×10^{10}-1.1×10^{12} molecules cm^{-3} s, respectively. They correspond to 0.4-14.2

133 and 0.6-8.5 equivalent days (photochemical age), respectively, assuming that an average OH concentration

134 in air is 1.5×10^6 molecules cm^{-3} (Mao et al., 2009).

135   Pure D3-D6 cVMS compounds (solid D3 and liquid D4, D5 and D6) were placed in a glass U-type tube

136 and maintained at room temperature. Vapors from these compounds (Table S1 of the Supplement) were

137 separately introduced into the ECCC-OFR by a small flow of zero air (1-18 mL min^{-1}) passing over the

138 headspace of the U-tube containing the pure compounds. The concentrations of D3-D6 in the ECCC-OFR

139 ranged from 20 to 43 ppb (Table S2), depending on their volatilities. Table S2 summarizes the concentrations

140 of cVMS at the reactor inlet and outlet, when the OH exposure was 1.85×10^{12} and 1.10×10^{12} molecules cm^{-}

141 ^{3} s in low and high-NO$_x$ experiments, respectively, indicating the reaction depth of cVMS. To study the

142 influence of existing particles on the SOA formation, ammonium sulfate (AS) seed particles were produced

143 using an atomizer, dried by a diffusion dryer and neutralized by a neutralizer and injected into the reactor

144 without size selection. The mass concentration of AS seed particles was approximately 30 μg m^{-3} for all

145 experiments.

146   N$_2$O was used as a source of NO to achieve high-NO$_x$ conditions (Lambe et al., 2017). NO$_x$ conditions

147 were defined by the fate of peroxy radicals (RO$_2$), which was described by the reaction rate ratio (R_{NO}) of

148 RO$_2$ + NO and RO$_2$ + HO$_2$ (Peng et al., 2018). The R_{NO} ratio increases with increasing OH exposures at a

149 constant concentration of N$_2$O (Li et al., 2019b). To achieve a constant branching ratio during the high-NO$_x$

150 experiments, the initial N$_2$O concentration in the OFR was varied (1.6%-8.0%) to maintain an R_{NO} value of

151 20 (Li et al., 2019b), as calculated using a model (OFR Exposures Estimator v3.1) (Peng et al., 2018). A

152 ratio of R_{NO}=20 indicates that 95% of RO$_2$ reacts with NO, ensuring the dominance of RO$_2$ + NO, which

153 represents conditions that are relevant for urban atmosphere (Peng et al., 2019). The role of RO$_2$ + RO$_2$ here

154 should be minor or negligible due to the low concentration of SOA precursors (cVMS, 18-46 ppb) (Lambe

155 et al., 2017; Peng et al., 2019; Li et al., 2019b). Peng et al. (2019) have reported that in the experiments

156 utilizing the injection of N_2O to achieve high-NO_x conditions, the relative importance of RO_2 + OH was

157 generally negatively correlated with N_2O due to the suppressing effect of NO_x on OH radicals and the

158 increasing role of RO_2 + NO. Under low-NO_x conditions, N_2O was not introduced into the OFR, where the

159 reaction ratio of RO_2 with HO_2 was estimated to be larger than 99% according to the model mentioned above

160 (Peng et al., 2018), representing atmospheric scenarios with few NO_x sources.

161 **2.2 Characterization and analysis**

162 The concentrations of cVMS in the OFR were measured online with PTR-ToF-MS (Ionicon Analytik

163 GmbH) (Liggio et al., 2016). The number and mass size distribution of aerosols was monitored using a

164 scanning mobility particle sizer (SMPS, TSI). The mass spectra and elemental composition of aerosols was

165 determined with a high-resolution time-of-flight aerosol mass spectrometer (HR-ToF-AMS, Aerodyne) and

166 analyzed with the AMS analysis software Squirrel (version 1.62G) and Pika (version 1.22G).

167 SOA mass yields (Y) were calculated via Equation 2,

168
$$Y = \frac{\Delta C_{\text{SOA}}}{\Delta C_{\text{cVMS}}} \tag{2}$$

169 where ΔC_{SOA} and ΔC_{cVMS} are the mass concentrations of SOA formed and cVMS lost, respectively. The mass

170 concentration of SOA was determined by multiplying the effective aerosol density by the integrated SOA

171 volume concentration from the SMPS, subtracting the AS seed volume for experiments with AS seeds. The

172 effective aerosol density (ρ) was calculated for unseeded experiments through the following Equation 3

173 (Lambe et al., 2015),

174
$$\rho = \frac{D_{va}}{D_m} \tag{3}$$

175 where D_{va} is the vacuum aerodynamic diameter obtained from the HR-ToF-AMS, and D_m is the electric

176 mobility diameter measured by the SMPS. The ρ varied in the range of 1.6-1.8 depending on the cVMS. The

177   same ρ value was also used in the seeded experiments. It should be pointed out that the background values

178   in Table S3 have been subtracted when calculating the cVMS SOA yields. The average data of SMPS and

179   AMS in the last ~10 minutes for each OH exposure was used to calculate the SOA yields (inset of Fig S2),

180   which can reduce the deviation caused by unstable SOA loadings at high OH exposures.

3 Results and discussion

3.1 SOA yields

183   Taking the D5 SOA under unseeded conditions as an example, the number and mass size distributions of

184   aerosols were shown in Fig. S3 at three photochemical ages (PA), i.e., time-integrated OH exposure. It can

185   be seen that small particles dominated the total particle number counts, while large ones dominated the mass.

186   The mass mode diameter of SOA for mass size distributions increased with PA under low and high-NO_x

187   conditions. The mass concentrations and time series of SOA obtained from SMPS and AMS were shown in

188   Table S4 and Fig. S2, respectively, which reflected a step-by-step pattern with increasing OH exposures.

189   Unstable SOA loadings at high OH exposures may be attributed to the fragmentation reactions, leading to

190   the difficulty in the deposition of products on SOA.

191   Figure 1 shows the SOA yields from the photooxidation of the D3-D6 cVMS under low and high-NO_x

192   conditions as a function of PA, with and without AS seed particles. SOA yields have been widely used to

193   estimate the potential of precursors to produce aerosol mass (Mcfiggans et al., 2019; Li et al., 2019a; Bruns

194   et al., 2015; Lambe et al., 2015). As shown in Fig. 1, the cVMS SOA yields exhibited an overall increasing

195   trend with PA, expressed in equivalent photochemical days, which agreed with the trend of D5 SOA yields

196   reported by Janechek et al. (2019). Under low-NO_x conditions (Fig. 1a), SOA yields exhibited a slow growth,

197   reaching a plateau after 10 equivalent days. This may be due to increased gas-phase fragmentation of cVMS

198   to generate some higher volatility products, leading to a small increasing amplitude of partition ratio of

199   species into SOA at longer photochemical ages.
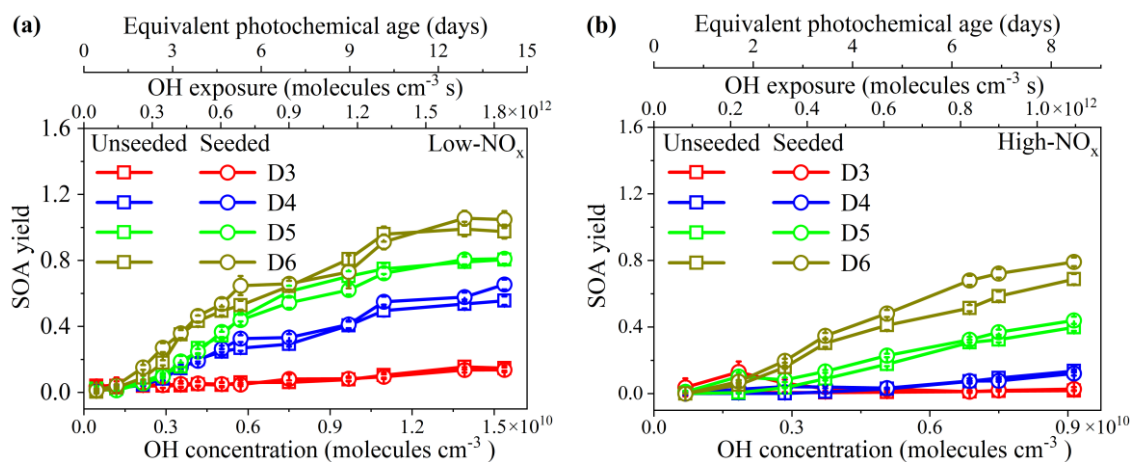
201   Figure 1. SOA yields from unseeded and seeded (30 μg m^{-3}) photooxidation of cVMS by OH radicals. (a)

202   low-NO$_x$ experiments; (b) high-NO$_x$ experiments.

203

204   For the unseeded and low-NO$_x$ experiments in Fig. 1a, SOA yields of four cVMS exhibited significant

205   differences in values over the same number of equivalent days. The SOA yields successively increased from

206   D3 to D6, consistent with the volatilities and molecular masses of the cVMS as well as their reaction rate

207   constants with the OH radical (Alton and Browne, 2020; Kim and Xu, 2017; Safron et al., 2015). The

208   maximum SOA yields of D3-D6 were (0.16±0.02), (0.56±0.03), (0.80±0.03) and (0.99±0.04), respectively,

209   occurring after a PA of 12 equivalent days. It has been reported that D5 SOA yields varied in the range of 0-

210   1.1 (Janechek et al., 2019; Wu and Johnston, 2017; Charan et al., 2022). Under a low OH exposure (~10^{10}-

211   10^{11} molecules cm^{-3} s), the D5 SOA yield (0.01-0.11) obtained here was similar to that (chamber, 0-0.057;

212   flow tube, 0.018-0.06) measured by Charan et al. (2022). However, under a high OH exposure of ~10^{11}-10^{12}

213   molecules cm^{-3} s, the D5 SOA yield of 0.46-0.70 was higher than 0.22 and 0.14-0.35 (flow tube) reported

214   by Janechek et al. (2019) and Charan et al. (2022), respectively, which may be attributed to differences in

215   experimental conditions, such as differences in reactors, wall losses, SOA measurement methods,

216   determination of OH concentrations, and initial D5 concentrations (Table S5) (Janechek et al., 2019; Charan

217   et al., 2022). Although the amount of cVMS lost was variable, cVMS SOA yields positively depended on

218   SOA mass concentrations (Fig. S4), and this trend was observed in previous D5 SOA experiments with OH

219   oxidation (Wu and Johnston, 2017).

220   As shown in Fig. 1b, the order of SOA yields from the four cVMS under high-NO_x conditions was the

221   same as that under low-NO_x conditions. However, the SOA yields under high-NO_x conditions were generally

222   smaller than the corresponding yields at similar OH exposures under low-NO_x conditions, with a decrease

223   of 0.05-0.30 depending on the cVMS. Such a reduction suggests that NO_x can restrict the formation of cVMS

224   SOA. NO_x has been shown to reduce SOA yields for some anthropogenic alkanes (Li et al., 2019b), aromatics

225   (Ng et al., 2007a; Chan et al., 2009; Zhou et al., 2019), monoterpenes (Zhao et al., 2018) and other terpenes

226   (Ng et al., 2007b), attributable to the formation of higher volatility products (e.g., organic nitrates) generated

227   by RO_2 + NO compared to RO_2 + HO_2 (Presto et al., 2005; Li et al., 2019b), which is also likely the case

228   here. The higher volatility products favor partitioning in the gas phase, thus reducing the potential for

229   forming SOA (Zhou et al., 2019). Moreover, high NO_x levels can suppress the formation of products for

230   nucleation, thereby reducing aerosol surface as a condensational sink and increasing the wall loss of

231   condensable species in an OFR under high-NO_x conditions (Zhao et al., 2018; Sarrafzadeh et al., 2016; Wildt

232   et al., 2014). Figure S5 indicates that the difference between SOA yields with and without NO_x decreased

233   with increasing silicon atoms within individual cVMS, indicating a less restricting effect of NO_x on the SOA

234   formation for larger cVMS. This means that high NO_x levels play a lessor role in the SOA yields of lower

235   volatility precursors.

236   SOA yields in the AS-seeded experiments under low and high-NO_x conditions are also shown in Figs. 1

237   and S5, indicating minimal impacts of the AS seed particles on SOA yields. A yield enhancement ratio

238   ($R_E = Y_{seeded}/Y_{unseeded}$, Fig. S6) was used to show the seed impacts more clearly. Under low-NO_x conditions,

239 the R_E values for all cVMS were close to 1.0 (Fig. S6a), suggesting a negligible impact of AS seed particles

240 on SOA yields; however, under high-NO$_x$ conditions, R_E was much larger (17.81, 13.18 and 15.51 for D3-

241 D5, respectively) at short PA but gradually decreased to 1.0 with increasing PA for D3-D5, while it was

242 always close to 1.0 for D6 regardless of PA (Fig. S6b). R_E values greater than 1.0 suggest that AS seed

243 particles played an enhancement role in the cVMS SOA formation, as similarly reported in SOA formation

244 from hydrocarbons (Sarrafzadeh et al., 2016; Lamkaddam et al., 2017; Li et al., 2019b). Under low-NO$_x$

245 conditions, the general lack of impact on cVMS SOA yields by the AS seed particles suggests that

246 condensation was not the main process driving SOA formation in cVMS oxidation. For the few cases of high

247 NO$_x$ level at low PA, where R$_E$ was >1 for D3-D5, it is possible that their early generations of oxidation

248 products were more volatile than successive generations of products and hence more prone to condensation

249 enhanced by AS seeds. As PA increased, further reactions of these early generation oxidation products with

250 OH radicals resulted in further generation products that were likely less volatile, thereby weakening the

251 enhancing role of AS seeds at high OH exposure. Such effect was less pronounced for D6, likely because its

252 oxidation products at different PA had similar volatilities. Figure S6b shows that the effect of AS seed

253 particles on SOA yields negatively correlated with the number of silicon atoms in the cVMS. Lower volatility

254 precursors (D5 and D6) may form lower volatile products, resulting in SOA yields less sensitive to the pre-

255 existing seeds.

256 **3.2 Aerosol compositions**

257 **3.2.1 Compositions of SOA under low-NO$_x$ conditions.**

258 Figures 2 and S7 show the normalized HR-ToF-AMS mass spectra of cVMS SOA from unseeded

259 experiments under low-NO$_x$ conditions at OH exposures of 9.0×10^{11} molecules cm^{-3} s (i.e., OH

260 concentration of 7.5×10^9 molecules cm^{-3}). The mass spectral signals can be identified as fragments with a

261   formula of $C_xH_yO_zSi_n$. For D3 SOA, the most prominent peaks were at m/z 44 and 29, dominated by CO_2^+

262   and CHO^+, which were tracers for organic acids (Ng et al., 2010), alcohols and aldehydes (Lee et al., 2012),

263   respectively. They may result from the oxidation of the methyl groups in D3 by OH radicals. For the mass

264   spectra of D4-D6 SOA, the two highest peaks at m/z 14 and 15 were CH_2^+ and CH_3^+, respectively. In addition,

265   there were several dominant $C_xH_yO_zSi_n$ peaks, which were fragments of silicon-containing products. For the

266      $C_xH_yO_zSi_n$ group in D4 SOA, there were four typical peaks at m/z 255, 257, 271 and 273, with formulae of

267      $C_4H_{11}O_7Si_3^+$, $C_3H_9O_8Si_3^+$, $C_3H_7O_9Si_3^+$ and $C_3H_9O_9Si_3^+$, respectively. The $C_xH_yO_zSi_n$ fragment group

268   containing Si of D5 SOA had three dominant peaks at m/z 327, 329 and 331, corresponding to $C_{12}H_{11}O_2Si_5^+$,

269      $C_9H_9O_8Si_3^+$ and $C_5H_{15}O_9Si_4^+$, respectively. For the $C_xH_yO_zSi_n$ group containing Si in D6 SOA, there were

270   five main peaks at m/z 73 (C_3H_9Si), 387 ($C_8H_{23}O_8Si_5^+$), 389 ($C_8H_9O_9Si_5^+$), 401 ($C_9H_{21}O_{10}Si_4^+$) and 403

271   ($C_7H_{15}O_{12}Si_4^+$).

272

273
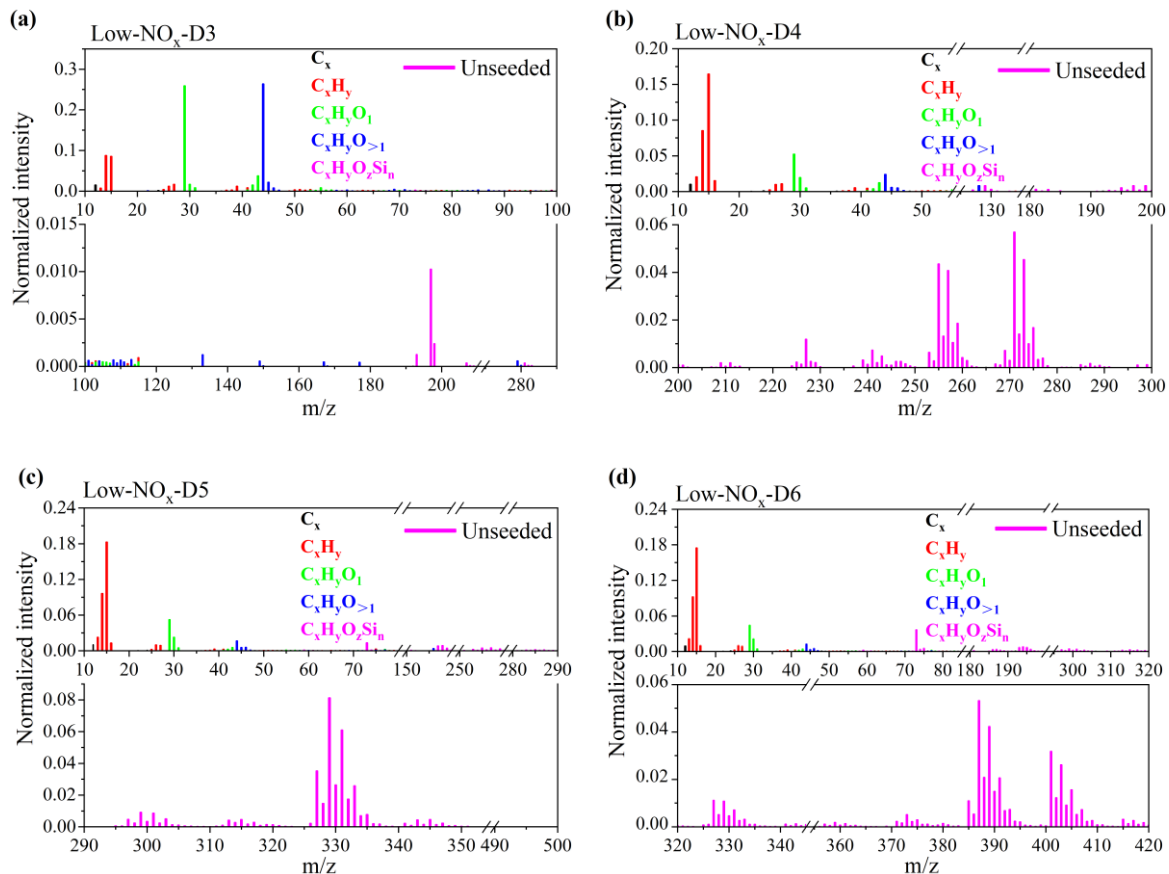
Figure 2. HR-ToF-AMS mass spectra of cVMS SOA at OH exposure of 9.0×10^{11} molecules cm^{-3} s (i.e.,

OH concentration of 7.5×10^9 molecules cm^{-3}) under low-NO$_x$ conditions in unseeded experiments. a-d

represent the mass spectra of D3-D6 SOA, respectively.

Figure 3 shows the evolution of different groups of ions in the HR-ToF-AMS spectra of the cVMS SOA

as a function of PA in equivalent days. For D3-D6 under unseeded conditions, $C_xH_yO_1$ and $C_xH_yO_{>1}$ ions

significantly decreased within 0-4 equivalent days of PA, but remained essentially unchanged when PA

increased to 7-15 equivalent days. The C_xH_y ion increased to its peak value at about 9 equivalent days of PA

for D3 and 2-3 equivalent days of PA for D4-D6, and then gradually decreased with further PA increases.

The $C_xH_yO_zSi_n$ group of ions maintained an increasing trend until 9-10 days of PA, thereafter it decreased

slightly for D4-D6 SOA.

285 The weighted values of the Si/C (n/x) and Si/O (n/z) atomic ratios for the $C_xH_yO_zSi_n$ groups in D5 and D6

286 SOA at different PA are plotted in Fig. S8 (Detailed calculations in Text S1 of the Supplement), which can

287 be used to indicate the changes in the Si element of SOA. The Si/C ratio increased slightly with increasing

288 PA, whereas the Si/O ratio had an overall decrease trend. While it is difficult to separate the effect of

289 fragmentation due to the AMS ionization process, the relative changes of group intensities and the evolution

290 of Si/C and Si/O in $C_xH_yO_zSi_n$ over different PA may be attributed to the evolution of cVMS when oxidized

291 by the OH radicals. The initial step of OH radical oxidation is H abstraction from the methyl groups on the

292 -Si-O- ring of the cVMS to form Si-containing radicals, which may generate OH and CH_2OH substitution

293 products, such as silanol and silyl methanol (Wu and Johnston, 2016; Alton and Browne, 2020). Such Si-

294 containing products may partition into SOA and result in an appearance of $C_xH_yO_zSi_n$ ions in the AMS mass

295 spectra. Notably, it was reported that one of oxidation products of D5, 1-

296 hydroxynonamethylcyclopentasiloxane (D_4TOH), has been detected in ambient particulate matter (Milani et

297 al., 2021). At low PA, some oxygen-containing functional groups (-CH_2OH/-COOH/-OH), which were

298 formed by the reaction of methyl groups in cVMS with OH, resulted in a decrease of Si/O ratio. The Si-O

299 bond breaking may mainly happen at high OH exposures, and it may occur after the cleavage of Si-C bonds

300 (Rücker and Kümmerer, 2015). According to the previous study of Wu and Johnston (2017), some ring-

301 opened products were generated from the reaction of D5 with OH radicals, necessarily requiring the cleavage

302 of Si-O bonds. The Si-O bond cleavage from the OH radical attack may reduce the number of Si atoms,

303 leading to a continuous decrease of Si/O at high PA. The continued breaking of Si-O bonds would lead to

304 fragmentation and more volatile products, which caused lower SOA yield and $C_xH_yO_zSi_n$ fraction at longer

305 PA (Figs. 1 and 3). The field measurements observed that Si acts as a frequent component of atmospheric

306 nanoparticles (Bzdek et al., 2014). This work further determines that cVMS SOA could become an important

307   contributor to Si in aerosols.
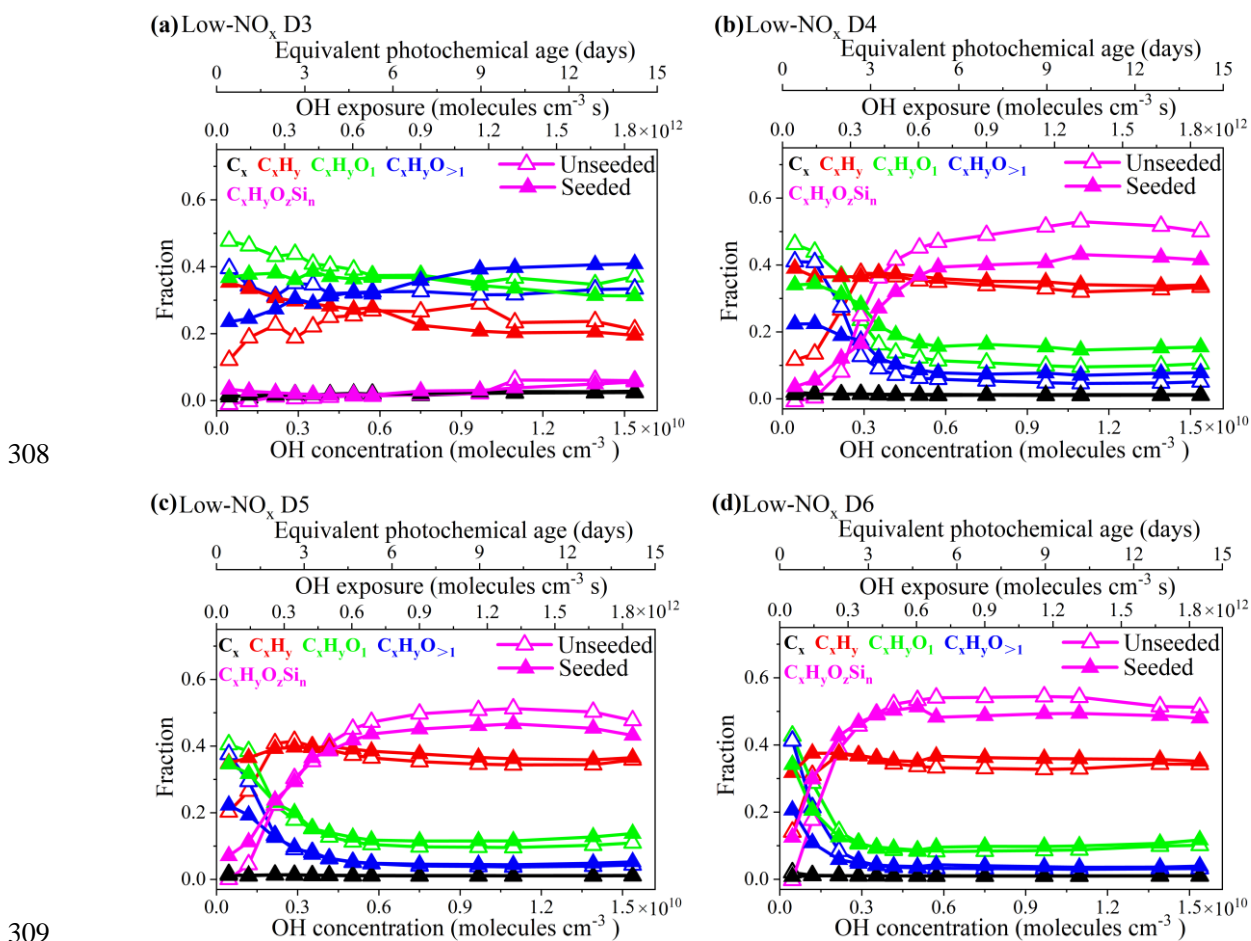
310   Figure 3. Fraction of C_x, C_xH_y, $C_xH_yO_1$, $C_xH_yO_{>1}$ and $C_xH_yO_zSi_n$ ion groups for SOA derived from the

311   oxidation of cVMS (a-d) by OH radicals at different photochemical ages under low-NO_x conditions.

312   Empty and solid triangles represent experimental data under unseeded and seeded conditions, respectively.

313

314   As shown in Fig. 3, the presence of seeds led to some changes in the evolution trends of ion groups in the

315   AMS spectra. For instance, the initial fraction of C_xH_y in seeded experiments was larger than that in unseeded

316   experiments, which may be related to the volatility of species containing C_xH_y that may be more easily

317   deposited in the presence of seeds, whereas $C_xH_yO_1$ and $C_xH_yO_{>1}$ exhibited opposite changes. The presence

318   of seeds led to larger initial and smaller steady-state $C_xH_yO_zSi_n$ fractions than those in unseeded experiments.

319   Regardless of the presence of seeds, C_xH_y, $C_xH_yO_1$ and $C_xH_yO_{>1}$ mainly contributed to the composition of

320   all cVMS SOA at initial OH radicals oxidation, but D4-D6 SOA primarily consisted of C_xH_y and $C_xH_yO_zSi_n$

321   after 4 equivalent days.

3.2.2 Compositions of SOA under high-NO$_x$ conditions.

323   Figure S9 shows the HR-ToF-AMS mass spectra of cVMS SOA from unseeded experiments under high-

324   NO$_x$ conditions at OH exposures of 9.0×10^{11} molecules cm^{-3} s (~6.9 d). Compared to that under low-NO$_x$

325   conditions (Figs. 2 and S7), there was one additional N-containing group (N_mO_z) in the SOA mass spectra

326   under high-NO$_x$ conditions, which accounted for 16%-31%. For the mass spectra of D3-D6 SOA originating

327   from unseeded experiments under high-NO$_x$ conditions in Fig. S9, the dominating peaks of the N_mO_z family

328   were m/z 30 (NO$^+$) and m/z 46 (NO$_2^+$). The common main peaks were located at m/z 30 (NO$^+$) for cVMS

329   SOA, m/z 44 (CO$_2^+$) for D3-D4 SOA, and m/z 46 (NO$_2^+$) for D4-D6 SOA. In addition, there were other

330   primary peaks at m/z 29 (CHO$^+$) for D4 SOA, while m/z 15 (CH$_3^+$) and m/z 28 (CO$^+$) for D5-D6 SOA. The

331   m/z 28 (CO$^+$), similar to m/z 44 (CO$_2^+$), is considered as a tracer for organic acids (Ng et al., 2010). In the

332   mass spectra for D3-D6 SOA under high-NO$_x$ conditions, the presence of NO$^+$ (m/z 30) and NO$_2^+$ (m/z 46)

333   illustrated the formation of organic or inorganic nitrates in SOA (Ng et al., 2007b; Zhao et al., 2018).

334   For the $C_xH_yO_zSi_n$ group in the D4 SOA mass spectrum under high-NO$_x$ conditions, the dominating peaks

335   and their formulas were the same as those under low-NO$_x$ conditions. For the $C_xH_yO_zSi_n$ group in D5 SOA,

336   in addition to two typical peaks at m/z 327 and 329 in the low-NO$_x$ experiments, there was another prominent

337   peak at m/z 328, with a formula $C_8H_{12}O_5Si_5$. The $C_xH_yO_zSi_n$ group in D6 SOA had three typical peaks at m/z

338   73 (C$_3$H$_9$Si), m/z 387 (C$_8$H$_{23}$O$_8$Si$_5^+$) and m/z 401 (C$_9$H$_{21}$O$_{10}$Si$_4^+$). For the $C_xH_yO_zSi_n$ groups in cVMS SOA,

339   there was little difference in the x, y, z and n value assignment of $C_xH_yO_zSi_n$ peaks in SOA generated under

340   low-NO$_x$ and high-NO$_x$ conditions, suggesting the formation of similar Si-containing oxidation products.

341   For cVMS SOA under high-NO$_x$ conditions, the evolution of family groups as a function of OH exposure

342 was summarized in Fig. S10. The dominant composition at the initial stage was $C_xH_yO_{>1}$ groups for D3-D6

343 SOA. At equivalent days larger than 4, D3 SOA primarily consisted of $C_xH_yO_{>1}$, N_mO_z and $C_xH_yO_1$ groups,

344 while D4-D6 SOA was mainly composed of $C_xH_yO_zSi_n$, N_mO_z, $C_xH_yO_1$, C_xH_y and $C_xH_yO_{>1}$ groups. Figure

345 S10 also shows influences of seeds on the evolution of family groups under high-NO_x conditions. It was

346 observed that all groups in D3-D6 SOA displayed similar change trends regardless of the existence of seeds.

347 As shown in Fig. S11, the trend of the Si/O ratio in the $C_xH_yO_zSi_n$ groups at different photochemical ages

348 under high-NO_x conditions was similar to that in low-NO_x experiments. However, the Si/C ratios remained

349 almost unchanged, and were close to the initial value (0.5) in cVMS. This may be attributed to the possible

350 suppression of cleavage of methyl groups from the -Si-O- ring of the cVMS under high-NO_x conditions.

4 Conclusions and implications

352 The yields and compositions of SOA generated from the photooxidation of four cVMS (D3-D6) with OH

353 radicals were investigated using an oxidation flow reactor. cVMS SOA yields exhibited an overall increasing

354 trend with PA, and their values gradually increased with cVMS from D3 to D6. SOA formations depended

355 on NO_x, as shown by smaller SOA yields under high-NO_x conditions. Ammonium sulfate seeds significantly

356 enhanced SOA yields of D3-D5 at short PA under high-NO_x conditions. The SOA mass spectra showed that

357 Si-containing species were one of main chemical compositions at PA > 4 days.

358 To evaluate the potential contributions of cVMS to SOA formation in the atmosphere, global SOA

359 concentrations produced from cVMS were estimated according to the cVMS SOA yields measured in this

360 work and using the cVMS concentrations reported from multiple studies, which were listed in Table S6.

361 Figure 4 shows the global concentration distribution of SOA from four cVMS (D3-D6) at 36 sites worldwide

362 estimated by the Equation 4,

$$C_{cVMS\text{-}SOA} = C_{cVMS} \times \frac{\Delta C_{cVMS}}{C_{in\text{-}cVMS}} \times Y \tag{4}$$

364 where C_{cVMS} and $C_{cVMS-SOA}$ are the mass concentration of cVMS reported from literatures and cVMS SOA

365 estimated in global sites, respectively; $C_{in-cVMS}$ and ΔC_{cVMS} are the mass concentration of initial and lost

366 cVMS at the selected equivalent days during the experiments of this work, respectively (Table S7); Y is the

367 cVMS SOA mass yields selected here. The estimations from the Equation 4 were based on assumptions that

368 the lost cVMS ratio is not affected by the cVMS concentration and the background $C_{cVMS-SOA}$ is zero. The

369 dilution of cVMS would occur during the transportation in the atmosphere, leading to an uncertainty of

370 cVMS concentrations (C_{cVMS}) in the Equation 4. To simplify the estimation process, the effect of dilution on

371 C_{cVMS} would not be taken into account, and the reported C_{cVMS} values were directly used. It was noted that

372 the time-integrated consumption over the lifetime of a precursor compound in the atmosphere should be

373 suitable for evaluating the SOA formation. Accordingly, when considering atmospheric half-lives (6-30 days)

374 of cVMS, the $\Delta C_{cVMS}/C_{in-cVMS}$ values in low-NO$_x$ and unseeded experiments at 14.2 equivalent days (Table

375 S7) are used to calculate cVMS SOA at background and polar sites. Due to a short residence time of airmass

376 over urban areas, the $\Delta C_{cVMS}/C_{in-cVMS}$ values in high-NO$_x$ and seeded experiments at 0.63 equivalent days

377 (Table S7) are employed to estimate cVMS SOA at urban sites.

378   It should be noted that OH concentrations and exposures have different effects on the reaction systems,

379 leading to different SOA yields. Under an ideal condition, a low OH concentration for a long exposure time

380 and a high OH concentration for a short exposure time can achieve the same degree of degradation of the

381 precursor compound. However, this is not applicable for the formation of SOA. Charan et al. (2022) have

382 claimed that D5 SOA yields are dependent on the OH concentrations rather than OH exposures. When

383 extrapolating the laboratory data to the real atmosphere, it is necessary to consider atmospherically relevant

384 OH concentrations and exposures. Charan et al. (2022) also stated that the D5 SOA yield varied in a small

385 range (0-6%) at the OH concentration $\leq 5 \times 10^8$ molecules cm^{-3}. It was assumed that the SOA yields at

386   environmentally relevant OH concentrations ($\sim 10^6$ molecules cm^{-3}) were similar to those at the lowest OH

387   concentrations ($\sim 10^8$ molecules cm^{-3}) used here. Thus, the high-NO$_x$ SOA yields (D3: 0.038; D4: 0.001; D5:

388   0.011; D6: 0.000) under the seeded conditions at the OH concentration of 6.83×10^8 molecules cm^{-3} (0.63

389   equivalent days) were employed in the calculation of cVMS SOA concentrations at urban sites, while the

390   low-NO$_x$ SOA yields (D3: 0.041; D4: 0.013; D5: 0.023; D6: 0.004) under the unseeded conditions at the OH

391   concentration of 4.57×10^8 molecules cm^{-3} (0.42 equivalent days) were used to estimate cVMS SOA at

392   background and polar sites. Although there may be some uncertainties in extrapolating our results to the real

393   atmosphere, these extrapolations may still provide an estimation for understanding the SOA potential of

394   cVMS.

395   Table S6 summarizes the details regarding sites and concentrations of cVMS SOA. The derived

396   concentrations of cVMS SOA vary significantly among urban, background and polar sites. The total cVMS

397   SOA concentrations in urban areas are the highest, up to 33.52 ng/m^3, which was comparable with the

398   maximum cVMS SOA formation (21 ng/m^3) reported by Pennington et al. (2021) using the CMAQ model

399   for Los Angeles. They are 0.57-8.86 and 0.37-1.97 ng/m^3 for background and Arctic sites, respectively.

400   cVMS SOA concentrations in urban regions of Asia (sites 29-36) and Europe (sites 26-28) are generally

401   larger than that of North America (sites 20-25). In China, the total cVMS SOA concentrations in urban sites

402   range from 0.11 to 33.52 ng/m^3. The main precursors of cVMS SOA are different among Chinese cities. For

403   three cities along the southeast coast of China (Guangzhou, Macau and Foshan), the dominant precursors of

404   cVMS SOA are D3 and D4, which are related to industrial emissions of these two siloxanes in this region

405   (Wang et al., 2001). For Dalian in China, D5 mainly contributes to cVMS SOA, and this can be attributed to

406   the industrial production and the use of personal care products in Dalian (Li et al., 2020). In the other Chinese

407   urban areas with reported cVMS concentrations (Lhasa, Golmud, Kunming and Yantai), the total cVMS

408 SOA concentrations are considerably smaller than those in the urban areas above, with D5 acting as the main

409 precursor, which may be ascribed to the relatively low population densities in these cities (Wang et al., 2018).
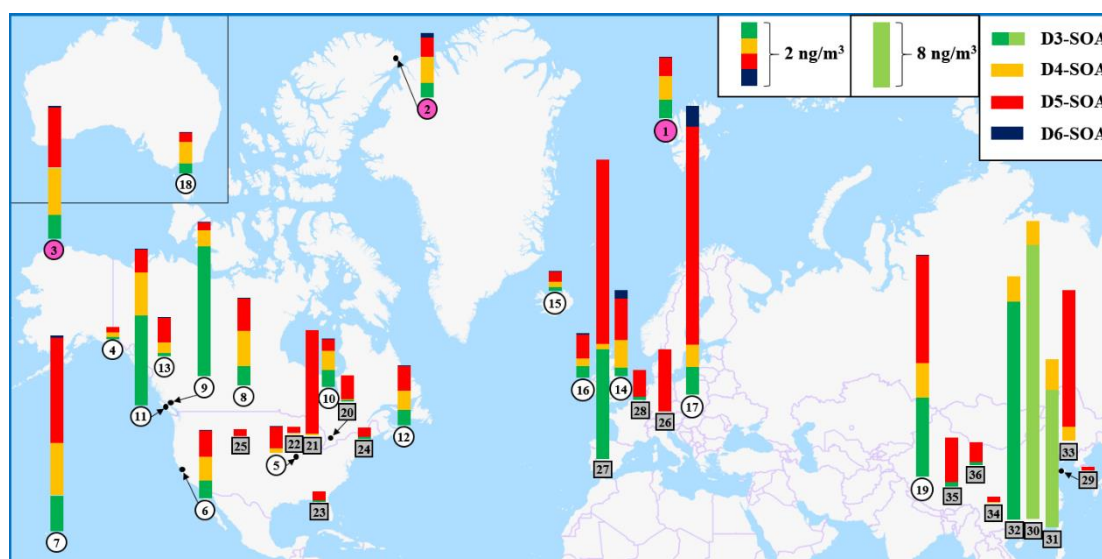
410

411 Figure 4. Global concentrations of cVMS SOA (ng/m³) on the basis of the cVMS concentrations

412 reported from multiple studies and the cVMS SOA yields measured in this work. The numbers of polar,

413 background and urban sites are enclosed in pink, white circles and gray boxes, respectively. The details

414 about cVMS and SOA concentrations at different sites were summarized in Table S6 of the Supplement.

415

416 At urban sites in Europe and North America, cVMS SOA concentrations are reported in the range of 0.91-

417 9.16 ng/m³ and 0.19-3.23 ng/m³, respectively. Among these cVMS, D5 is the main contributor to cVMS

418 SOA at these locations, averaging 89.1% of total cVMS SOA. For instance, D5 SOA is calculated to be 5.63

419 ng/m³ in Catalan, Spain, 3.19 ng/m³ in Chicago, USA, 1.89 ng/m³ in Zurich, Switzerland and 0.81 ng/m³ in

420 Paris, France, where there are high levels of economic activities and high population densities. These results

421 suggest that personal care products as a main source of D5 may be the most important anthropogenic origins

422 of Si-containing SOA in Europe and North America. The D5 SOA concentration (0.11-5.63 ng/m³) estimated

423 here is larger than that (0.016-0.206 ng/m³) reported by Milani et al. (2021), who obtained their data using

424   semi-quantified concentrations of D_4TOH (first-generation D5 SOA product) extracted from $PM_{2.5}$ samples

425   in Atlanta and Houston. The difference may be mainly attributed to the missing analysis of multi-generation

426   SOA products or dimers (Wu and Johnston, 2016, 2017).

427   At background and Arctic sites, cVMS SOA are primarily derived from D3, D4 and D5. The background

428   sites are located in mountains, rural areas, forested areas, lakes and at high altitudes. The three highest cVMS

429   SOA concentrations at background sites are located at Kosetice in the Czech Republic (8.86 ng/m^3), Tibetan

430   Plateau in China (6.78 ng/m^3) and Hilo of Hawaii in the USA (5.97 ng/m^3), where the contribution

431   percentages of SOA from D3-D5 are 92.8%, 99.9% and 99.0%, respectively. The cVMS SOA concentrations

432   at the Alert site in Nunavut, Canada is the highest (1.97 ng/m^3) among the three locations in the Arctic, 92.4%

433   of which is accounted for by D3-D5 SOA. The dominance of D3-D5 SOA in both background and the Arctic

434   regions highlights their persistence in the atmosphere and the potential for long-range atmospheric transport.

435   The global annual production of D4, D5 and D6 is about 1, 0.1 and 0.01 $Tg \cdot yr^{-1}$, respectively, and 90% of

436   these cVMS is eventually released into the atmosphere (Li et al., 2020; Genualdi et al., 2011; Wang et al.,

437   2013; Sakurai et al., 2019). Based on the results shown in Fig. 4, the annual production of cVMS (D4-D6)

438   SOA was estimated to be 0.01 $Tg \cdot yr^{-1}$, which was about 0.34% of SOA (2.9 $Tg \cdot yr^{-1}$) produced from mobile

439   source emissions in the USA and 33%-50% of SOA generated by Athabasca oil sands (0.02-0.03 $Tg \cdot yr^{-1}$,

440   one of the largest sources of anthropogenic secondary organic aerosols in North America) (Tkacik et al.,

441   2014; Liggio et al., 2016). Moreover, it was 0.05% and 0.14% of isoprene-SOA (20 $Tg \cdot yr^{-1}$) and

442   monoterpenes-SOA (7 $Tg \cdot yr^{-1}$) (typical biogenic SOA), respectively, indicating the potential importance of

443   cVMS SOA (Jokinen et al., 2015). While these cVMS SOA sources may seem small, they can make

444   substantially higher contributions to ambient air SOAs in population centers where cVMS compounds are

445   primarily used.

446

Author contributions

CH designed and conducted all experiments; CH and HY analyzed the data and prepared the paper with

contributions from KL, PL, JL, AL and SML. SML supervised the project.

450

Competing interests

The authors declare that they have no conflict of interest.

453

Acknowledgements

This project was supported by Environment and Climate Change Canada's Climate and Clean Air Program

(CCAP); the National Natural Science Foundation of China (42077198); the LiaoNing Revitalization Talents

Program (XLYC1907185); the Fundamental Research Funds for the Central Universities (N2025011).

458

References

Ahrens, L., Harner, T., and Shoeib, M.: Temporal Variations of Cyclic and Linear Volatile Methylsiloxanes in the
   Atmosphere Using Passive Samplers and High-Volume Air Samplers, Environ. Sci. Technol., 48, 9374-9381,
   https://doi.org/10.1021/es502081j, 2014.

Allen, R., Kochs, P., and Chandra, G.: Industrial Organosilicon Materials, Their Environmental Entry and
   Predicted Fate, Springer, 3, 1-25, https://doi.org/10.1007/978-3-540-68331-5_1, 1997.

Alton, M. and Browne, E.: Atmospheric Chemistry of Volatile Methyl Siloxanes: Kinetics and Products of
   Oxidation by OH Radicals and Cl Atoms, Environ. Sci. Technol., 54, 5992-5999,
   https://dx.doi.org/10.1021/acs.est.0c01368, 2020.

Atkinson, R.: Kinetics of the Gas-Phase Reactions of a Series of Organosilicon Compounds with OH and NO_3
   Radicals and O_3 at 297 ± 2 K, Environ. Sci. Technol., 25, 863-866, https://doi.org/10.1021/es00017a005, 1991.

Bein, K., Zhao, Y., Wexler, A., Johnston, M.: Speciation of Size-Resolved Individual Ultrafine Particles in

Pittsburgh, Pennsylvania, J. Geophys. Res., 110, D07S05, https://doi.org/10.1029/2004jd004708, 2005.

Berndt, T., Richters, S., Jokinen, T., Hyttinen, N., Kurtén, T., Otkjaer, R., Kjaergaard, H., Stratmann, F., Herrmann, H., Sipilä, M., Kulmala, M., and Ehn, M.: Hydroxyl Radical-Induced Formation of Highly Oxidized Organic Compounds, Nat. Commun., 7, 1-8, https://doi.org/10.1038/ncomms13677, 2016.

Bruns, E., Haddad, I., Keller, A., Klein, F., Kumar, N., Pieber, S., Corbin, J., Slowik, J., Brune, W., Baltensperger, U., and Prévôt, A.: Inter-Comparison of Laboratory Smog Chamber and Flow Reactor Systems on Organic Aerosol Yield and Composition, Atmos. Meas. Tech., 8, 2315-2332, https://doi.org/10.5194/amt-8-2315-2015, 2015.

Bzdek, B., Horan, A., Pennington, M., Janechek, N., Baek, J., Stanier, C., and Johnston, M.: Silicon is a Frequent Component of Atmospheric Nanoparticles, Environ. Sci. Technol., 48, 11137-11145, https://doi.org/10.1021/es5026933, 2014.

Canada, E. C. a. H.: https://www.ec.gc.ca/ese-ees/FC0D11E7-DB34-41AA-B1B3-E66EFD8813F1/batch2_540-97-6_en.pdf last access: 9 February 2022, 2008.

Chan, A., Kautzman, K., Chhabra, P., Surratt, J., Chan, M., Crounse, J., Kürten, A., Wennberg, P., Flagan, R., and Seinfeld, J.: Secondary Organic Aerosol Formation from Photooxidation of Naphthalene and Alkylnaphthalenes: Implications for Oxidation of Intermediate Volatility Organic Compounds (IVOCs), Atmos. Chem. Phys., 9, 3049–3060, https://doi.org/10.5194/acp-9-3049-2009, 2009.

Chandramouli, B., Kamens, R.: The Photochemical Formation and Gas-Particle Partitioning of Oxidation Products of Decamethyl Cyclopentasiloxane and Decamethyl Tetrasiloxane in the Atmosphere, Atmos. Environ., 35, 87-95, https://doi.org/10.1016/S1352-2310(00)00289-2, 2001.

Charan, S., Huang, Y., Buenconsejo, R., Li, Q., Cocker Iii, D., and Seinfeld, J.: Secondary Organic Aerosol Formation from the Oxidation of Decamethylcyclopentasiloxane at Atmospherically Relevant OH Concentrations, Atmos. Chem. Phys., 22, 917-928, https://doi.org/10.5194/acp-22-917-2022, 2022.

Coggon, M., McDonald, B., Vlasenko, A., Veres, P., Bernard, F., Koss, A., Yuan, B., Gilman, J., Peischl, J., Aikin, K., DuRant, J., Warneke, C., Li, S.-M., and Gouw, J.: Diurnal Variability and Emission Pattern of Decamethylcyclopentasiloxane (D5) from the Application of Personal Care Products in Two North American Cities, Environ. Sci. Technol., 52, 5610-5618, https://doi.org/10.1021/acs.est.8b00506, 2018.

EUR-Lex: https://eur-lex.europa.eu/legal-content/EN/TXT/?uri=uriserv:OJ.L_.2018.006.01.0045.01.ENG&toc=OJ:L:2018:006:TOCECHA, last access: 25 November 2021, 2018.

501   Farasani, A. and Darbre, P.: Exposure to Cyclic Volatile Methylsiloxanes (cVMS) Causes Anchorage-Independent

502   Growth and Reduction of BRCA1 in Non-Transformed Human Breast Epithelial Cells, J. Appl. Toxicol., 37,

503   454-461, https://doi.org/10.1002/jat.3378, 2017.

504   Genualdi, S., Harner, T., Cheng, Y., Macleod, M., Hansen, K., Egmond, R., Shoeib, M., and Lee, S.: Global

505   Distribution of Linear and Cyclic Volatile Methyl Siloxanes in Air, Environ. Sci. Technol., 45, 3349-3354,

506   https://doi.org/10.1021/es200301j, 2011.

507   Glasius, M. and Goldstein, A.: Recent Discoveries and Future Challenges in Atmospheric Organic Chemistry,

508   Environ. Sci. Technol., 50, 2754-2764, https://doi.org/10.1021/acs.est.5b05105, 2016.

509   Guo, J., Zhou, Y., Cui, J., Zhang, B., and Zhang, J.: Assessment of Volatile Methylsiloxanes in Environmental

510   Matrices and Human Plasma, Sci. Total. Environ., 668, 1175-1182,

511   https://doi.org/10.1016/j.scitotenv.2019.03.092, 2019.

512   Huang, Y., Coggon, M., Zhao, R., Lignell, H., Bauer, M., Flagan, R., and Seinfeld, J.: The Caltech Photooxidation

513   Flow Tube reactor: Design, Fluid Dynamics and Characterization, Atmos. Meas. Tech., 10, 839-867,

514   https://doi.org/10.5194/amt-10-839-2017, 2017.

515   Janechek, N., Hansen, K., and Stanier, C.: Comprehensive Atmospheric Modeling of Reactive Cyclic Siloxanes

516   and their Oxidation Products, Atmos. Chem. Phys., 17, 8357-8370, https://doi.org/10.5194/acp-17-8357-2017,

517   2017.

518   Janechek, N., Marek, R., Bryngelson, N., Singh, A., Bullard, R., Brune, W., and Stanier, C.: Physical Properties

519   of Secondary Photochemical Aerosol from OH Oxidation of a Cyclic Siloxane, Atmos. Chem. Phys., 19, 1649-

520   1664, https://doi.org/10.5194/acp-19-1649-2019, 2019.

521   Jokinen, T., Berndt, T., Makkonen, R., Kerminen, V., Junninen, H., Paasonen, P., Stratmann, F., Herrmann, H.,

522   Guenther, A., Worsnop, D., Kulmala, M., Ehn, M., and Sipilä, M.: Production of Extremely Low Volatile

523   Organic Compounds from Biogenic Emissions: Measured Yields and Atmospheric Implications, Proc. Natl.

524   Acad. Sci. U S A., 112, 7123-7128, https://doi.org/10.1073/pnas.1423977112, 2015.

525   Kierkegaard, A. and McLachlan, M.: Determination of Linear and Cyclic Volatile Methylsiloxanes in Air at a

526   Regional Background Site in Sweden, Atmos. Environ., 80, 322-329,

527   https://doi.org/10.1016/j.atmosenv.2013.08.001, 2013.

528   Kim, J. and Xu, S.: Quantitative Structure-Reactivity Relationships of Hydroxyl Radical Rate Constants for Linear

529   and Cyclic Volatile Methylsiloxanes, Environ. Toxicol. Chem., 36, 3240-3245, https://doi.org/10.1002/etc.3914,

530   2017.

531   Kim, J., Mackay, D., and Whelan, M.: Predicted Persistence and Response Times of Linear and Cyclic Volatile

532   Methylsiloxanes in Global and Local Environments, Chemosphere, 195, 325-335,

533   https://doi.org/10.1016/j.chemosphere.2017.12.071, 2018.

534   Krogseth, I., Zhang, X., Lei, Y., Wania, F., and Breivik, K.: Calibration and Application of a Passive Air Sampler

535   (XAD-PAS) for Volatile Methyl Siloxanes, Environ. Sci. Technol., 47, 4463-4470,

536   https://doi.org/10.1021/es400427h, 2013a.

537   Krogseth, I., Kierkegaard, A., McLachlan, M., Breivik, K., Hansen, K., and Schlabach, M.: Occurrence and

538   Seasonality of Cyclic Volatile Methyl Siloxanes in Arctic Air, Environ. Sci. Technol., 47, 502-509,

539   https://doi.org/10.1021/es3040208, 2013b.

540   Lambe, A., Chhabra, P., Onasch, T., Brune, W., Hunter, J., Kroll, J., Cummings, M., Brogan, J., Parmar, Y.,

541   Worsnop, D., Kolb, C., and Davidovits, P.: Effect of Oxidant Concentration, Exposure Time, and Seed Particles

542   on Secondary Organic Aerosol Chemical Composition and Yield, Atmos. Chem. Phys., 15, 3063-3075,

543   https://doi.org/10.5194/acp-15-3063-2015, 2015.

544   Lambe, A., Ahern, A., Williams, L., Slowik, J., Wong, J., Abbatt, J., Brune, W., Ng, N., Wright, J., Croasdale, D.,

545   Worsnop, D., Davidovits, P., and Onasch, T.: Characterization of Aerosol Photooxidation Flow Reactors:

546   Heterogeneous Oxidation, Secondary Organic Aerosol Formation and Cloud Condensation Nuclei Activity

547   Measurements, Atmos. Meas. Tech., 4, 445-461, https://doi.org/10.5194/amt-4-445-2011, 2011.

548   Lambe, A., Massoli, P., Zhang, X., Canagaratna, M., Nowak, J., Daube, C., Yan, C., Nie, W., Onasch, T., Jayne,

549   J., Kolb, C., Davidovits, P., Worsnop, D., and Brune, W.: Controlled Nitric Oxide Production via O(^{1}D) + N_2O

550   Reactions for Use in Oxidation Flow Reactor Studies, Atmos. Meas. Tech., 10, 2283-2298,

551   https://doi.org/10.5194/amt-10-2283-2017, 2017.

552   Lamkaddam, H., Gratien, A., Pangui, E., Cazaunau, M., Varrault, B., and Doussin, J.: High-NO_x Photooxidation

553   of n-Dodecane: Temperature Dependence of SOA Formation, Environ Sci Technol, 51, 192-201,

554   https://doi.org/10.1021/acs.est.6b03821, 2017.

555   Lee, A., Hayden, K., Herckes, P., Leaitch, W., Liggio, J., Macdonald, A., and Abbatt, J.: Characterization of

556   Aerosol and Cloud Water at a Mountain Site During WACS 2010: Secondary Organic Aerosol Formation

557   through Oxidative Cloud Processing, Atmos. Chem. Phys., 12, 7103-7116, https://doi.org/10.5194/acp-12-

558   7103-2012, 2012.

559   Li, K., Liggio, J., Lee, P., Han, C., Liu, Q., and Li, S.-M.: Secondary Organic Aerosol Formation from α-Pinene,

560   Alkanes, and Oil Sand-Related Precursors in a New Oxidation Flow Reactor, Atmos. Chem. Phys., 19, 9715-

561   9731, https://doi.org/10.5194/acp-19-9715-2019, 2019a.

562   Li, K., Liggio, J., Han, C., Liu, Q., Moussa, S., Lee, P., and Li, S.-M.: Understanding the Impact of High-NO$_x$

563   Conditions on the Formation of Secondary Organic Aerosol in the Photooxidation of Oil Sand-Related

564   Precursors, Environ. Sci. Technol., 53, 14420-14429, https://doi.org/10.1021/acs.est.9b05404, 2019b.

565   Li, Q., Lan, Y., Liu, Z., Wang, X., Wang, X., Hu, J., and Geng, H.: Cyclic Volatile Methylsiloxanes (cVMSs) in

566   the Air of the Wastewater Treatment Plants in Dalian, China-Levels, Emissions, and Trends, Chemosphere, 256,

567   1-8, https://doi.org/10.1016/j.chemosphere.2020.127064, 2020.

568   Li, S.-M. and Winchester, J.: Particle Size Distribution and Chemistry of Late Winter Arctic Aerosols, J. Geophys.

569   Res., 95, 13897-13908, https://doi.org/10.1029/J095iD09p13897, 1990.

570   Li, S.-M. and Winchester, J.: Aerosol Silicon and Associated Elements in the Arctic High and Mid-Troposphere,

571   Atmos. Environ., 27, 2907-2912, https://doi.org/10.1016/0960-1686(93)90322-P, 1993.

572   Liggio, J., Li, S.-M., Hayden, K., Taha, Y., Stroud, C., Darlington, A., Drollette, B., Gordon, M., Lee, P., Liu, P.,

573   Leithead, A., Moussa, S., Wang, D., Brien, J., Mittermeier, R., Brook, J., Lu, G., Staebler, R., Han, Y., Tokarek,

574   T., Osthoff, H., Makar, P., Zhang, J., Plata, D., and Gentner, D.: Oil Sands Operations as a Large Source of

575   Secondary Organic Aerosols, Nature, 534, 91-94, https://doi.org/10.1038/nature17646, 2016.

576   Liu, N., Xu, L., and Cai, Y.: Methyl Siloxanes in Barbershops and Residence Indoor Dust and the Implication for

577   Human Exposures, Sci. Total. Environ., 618, 1324-1330, https://doi.org/10.1016/j.scitotenv.2017.09.250, 2018.

578   Mao, J., Ren, X., Brune, W., Olson, J., Crawford, J., Fried, A., Huey, L., Cohen, R., Heikes, B., Singh, H., Blake,

579   D., Sachse, G., Diskin, G., Hall, S., and Shetter, R.: Airborne Measurement of OH Reactivity during INTEX-

580   B, Atmos. Chem. Phys., 9, 163-173, https://doi.org/10.5194/acp-9-163-2009, 2009.

581   McFiggans, G., Mentel, T., Wildt, J., Pullinen, I., Kang, S., Kleist, E., Schmitt, S., Springer, M., Tillmann, R., Wu,

582   C., Zhao, D., Hallquist, M., Faxon, C., Breton, M., Hallquist, A., Simpson, D., Bergström, R., Jenkin, M., Ehn,

583   M., Thornton, J., Alfarra, M., Bannan, T., Percival, C., Priestley, M., Topping, D., and Scharr, A.: Secondary

584   Organic Aerosol Reduced by Mixture of Atmospheric Vapours, Nature, 565, 587-593,

585   https://doi.org/10.1038/s41586-018-0871-y, 2019.

586   Milani, A., Al-Naiema, I., and Stone, E.: Detection of a Secondary Organic Aerosol Tracer Derived from Personal

587   Care Products, Atmos. Environ., 246, https://doi.org/10.1016/j.atmosenv.2020.118078, 2021.

588   Ng, N., Kroll, J., Chan, A., Chhabra, P., Flagan, R., and Seinfeld, J.: Secondary Organic Aerosol Formation from

589   m-Xylene, Toluene, and Benzene, Atmos. Chem. Phys., 7, 3909–3922, https://doi.org/10.5194/acp-7-3909-

590   2007, 2007a.

591   Ng, N., Chhabra, P., Chan, A., Surratt, J., Kroll, J., Kwan, A., McCabe, D., Wennberg, P., Sorooshian, A., Murphy,

592   S., Dalleska, N., Flagan, R., and Seinfeld, J.: Effect of NO_x Level on Secondary Organic Aerosol (SOA)

593   Formation from the Photooxidation of Terpenes, Atmos. Chem. Phys., 7, 5159–5174,

594   https://doi.org/10.5194/acp-7-5159-2007, 2007b.

595   Ng, N., Canagaratna, M., Zhang, Q., Jimenez, J., Tian, J., Ulbrich, I., Kroll, J., Docherty, K., Chhabra, P., Bahreini,

596   R., Murphy, S., Seinfeld, J., Hildebrandt, L., Donahue, N., DeCarlo, P., Lanz, V., Prévôt, A., Dinar, E., Rudich,

597   Y., and Worsnop, D.: Organic Aerosol Components Observed in Northern Hemispheric Datasets from Aerosol

598   Mass Spectrometry, Atmos. Chem. Phys., 10, 4625-4641, https://doi.org/10.5194/acp-10-4625-2010, 2010.

599   Peng, Z., Taylor, J., Orlando, J., Tyndall, G., and Jimenez, J.: Organic Peroxy Radical Chemistry in Oxidation

600   Flow Reactors and Environmental Chambers and their Atmospheric Relevance, Atmos. Chem. Phys., 19, 813-

601   834, https://doi.org/10.5194/acp-19-813-2019, 2019.

602   Peng, Z., Palm, B., Day, D., Talukdar, R., Hu, W., Lambe, A., Brune, W., and Jimenez, J.: Model Evaluation of

603   New Techniques for Maintaining High-NO Conditions in Oxidation Flow Reactors for the Study of OH-

604   Initiated Atmospheric Chemistry, ACS. Earth. Space. Chem. , 2, 72-86,

605   https://doi.org/10.1021/acsearthspacechem.7b00070, 2018.

606   Pennington, E., Seltzer, K., Murphy, B., Qin, M., Seinfeld, J., and Pye, H.: Modeling Secondary Organic Aerosol

607   Formation from Volatile Chemical Products, Atmos. Chem. Phys., 21, 18247-18261,

608   https://doi.org/10.5194/acp-21-18247-2021, 2021.

609   Phares, D., Rhoads, K., Johnston, M., and Wexler, A.: Size-Resolved Ultrafine Particle Composition Analysis 2.

610   Houston, J. Geophys. Res., 108, 1-14, https://doi.org/10.1029/2001jd001212, 2003.

611   Presto, A., Hartz, K., and Donahue, N.: Secondary Organic Aerosol Production from Terpene Ozonolysis. 2. Effect

612   of NO_x Concentration, Environ. Sci. Technol. , 39, 7046-7054, https://doi.org/10.1021/es050400s, 2005.

613   Rauert, C., Shoieb, M., Schuster, J., Eng, A., and Harner, T.: Atmospheric Concentrations and Trends of Poly- and

614   Perfluoroalkyl Substances (PFAS) and Volatile Methyl Siloxanes (VMS) over 7 Years of Sampling in the Global

615   Atmospheric Passive Sampling (GAPS) Network, Environ. Pollut., 238, 94-102,

616   https://doi.org/10.1016/j.envpol.2018.03.017, 2018.

617   Rhoads, K., Phares, D., Wexler, A., Johnston, M.: Size-Resolved Ultrafine Particle Composition Analysis 1.

618   Atlanta, J. Geophys. Res., 108, 1-13, https://doi.org/10.1029/2001jd001211, 2003.

619   Riipinen, I., Juuti, T., Pierce, J., Petäjä, T., Worsnop, D., Kulmala, M., and Donahue, N.: The Contribution of

620   Organics to Atmospheric Nanoparticle Growth, Nat. Geosci., 5, 453-458, https://doi.org/10.1038/ngeo1499,

621 2012.

622 Rücker, C. and Kümmerer, K.: Environmental Chemistry of Organosiloxanes, Chem. Rev., 115, 466-524,

623 https://doi.org/10.1021/cr500319v, 2015.

624 Safron, A., Strandell, M., Kierkegaard, A., and Macleod, M.: Rate Constants and Activation Energies for Gas-

625 Phase Reactions of Three Cyclic Volatile Methyl Siloxanes with the Hydroxyl Radical, Int. J. Chem. Kinet., 47,

626 420-428, https://doi.org/10.1002/kin.20919, 2015.

627 Sakurai, T., Imaizumi, Y., Kuroda, K., Hayashi, T., and Suzuki, N.: Georeferenced multimedia environmental fate

628 of volatile methylsiloxanes modeled in the populous Tokyo Bay catchment basin, Sci Total Environ, 689, 843-

629 853, https://doi.org/10.1016/j.scitotenv.2019.06.462, 2019.

630 Sarrafzadeh, M., Wildt, J., Pullinen, I., Springer, M., Kleist, E., Tillmann, R., Schmitt, S., Wu, C., Mentel, T., Zhao,

631 D., Hastie, D., and Scharr, A.: Impact of NO_x and OH on Secondary Organic Aerosol Formation from β-Pinene

632 Photooxidation, Atmos. Chem. Phys., 16, 11237-11248, https://doi.org/10.5194/acp-16-11237-2016, 2016.

633 Simonen, P., Saukko, E., Karjalainen, P., Timonen, H., Bloss, M., Saksa, P., Rönkkö, T., Keskinen, J., and Maso,

634 M.: A New Oxidation Flow Reactor for Measuring Secondary Aerosol Formation of Rapidly Changing

635 Emission Sources, Atmos. Meas. Tech., 10, 1519-1537, https://doi.org/10.5194/amt-10-1519-2017, 2017.

636 Sommerlade, R., Parlar, H., Wrobel, D , Kochs, P.: Product Analysis and Kinetics of the Gas-Phase Reactions of

637 Selected Organosilicon Compounds with OH Radicals Using a Smog Chamber-Mass Spectrometer System,

638 Environ. Sci. Technol., 27, 2435-2440, https://doi.org/10.1021/es00048a019, 1993.

639 Tang, X., Misztal, P., Nazaroff, W., and Goldstein, A.: Siloxanes Are the Most Abundant Volatile Organic

640 Compound Emitted from Engineering Students in a Classroom, Environ. Sci. Technol. Lett. , 2, 303-307,

641 https://doi.org/10.1021/acs.estlett.5b00256, 2015.

642 Tkacik, D., Lambe, A., Jathar, S., Li, X., Presto, A., Zhao, Y., Blake, D., Meinardi, S., Jayne, J., Croteau, P., and

643 Robinson, A.: Secondary Organic Aerosol Formation from in-Use Motor Vehicle Emissions Using a Potential

644 Aerosol Mass Reactor, Environ. Sci. Technol., 48, 11235-11242, https://doi.org/10.1021/es502239v, 2014.

645 Wang, D.-G., Norwood, W., Alaee, M., Byer, J., and Brimble, S.: Review of Recent Advances in Research on the

646 Toxicity, Detection, Occurrence and Fate of Cyclic Volatile Methyl Siloxanes in the Environment, Chemosphere,

647 93, 711-725, https://doi.org/10.1016/j.chemosphere.2012.10.041, 2013.

648 Wang, X., Schuster, J., Jones, K., and Gong, P.: Occurrence and Spatial Distribution of Neutral Perfluoroalkyl

649 Substances and Cyclic Volatile Methylsiloxanes in the Atmosphere of the Tibetan Plateau, Atmos. Chem. Phys.,

650 18, 8745-8755, https://doi.org/10.5194/acp-18-8745-2018, 2018.

651 Wang, X., Lee, S., Sheng, G., Chan, L., Fu, J., Li, X., Min, Y., and Chan, C.: Cyclic organosilicon compounds in
652   ambient air in Guangzhou, Macau and Nanhai, Pearl River Delta, Appl. Geochemistry, 16, 1447-1454,
653   https://doi.org/10.1016/S0883-2927(01)00044-0, 2001.

654 Wildt, J., Mentel, T., Scharr, A., Hoffmann, T., Andres, S., Ehn, M., Kleist, E., Müsgen, P., Rohrer, F., Rudich, Y.,
655   Springer, M., Tillmann, R., and Wahner, A.: Suppression of New Particle Formation from Monoterpene
656   Oxidation by NO_x, Atmos. Chem. Phys., 14, 2789-2804, https://doi.org/10.5194/acp-14-2789-2014, 2014.

657 Wu, Y. and Johnston, M.: Molecular Characterization of Secondary Aerosol from Oxidation of Cyclic
658   Methylsiloxanes, J. Am. Soc. Mass Spectrom., 27, 402-409, https://doi.org/10.1007/s13361-015-1300-1, 2016.

659 Wu, Y. and Johnston, M.: Aerosol Formation from OH Oxidation of the Volatile Cyclic Methyl Siloxane (cVMS)
660   Decamethylcyclopentasiloxane, Environ. Sci. Technol., 51, 4445-4451,
661   https://doi.org/10.1021/acs.est.7b00655, 2017.

662 Xiao, R., Zammit, I., Wei, Z., Hu, W.-P., MacLeod, M., and Spinney, R.: Kinetics and Mechanism of the Oxidation
663   of Cyclic Methylsiloxanes by Hydroxyl Radical in the Gas Phase: An Experimental and Theoretical Study,
664   Environ. Sci. Technol., 49, 13322-13330, https://doi.org/10.1021/acs.est.5b03744, 2015.

665 Xu, S., Warner, N., Nizzetto, P., Durham, J., and McNett, D.: Long-Range Transport Potential and Atmospheric
666   Persistence of Cyclic Volatile Methylsiloxanes Based on Global Measurements, Chemosphere, 228, 460-468,
667   https://doi.org/10.1016/j.chemosphere.2019.04.130, 2019.

668 Zhao, D., Schmitt, S., Wang, M., Acir, I., Tillmann, R., Tan, Z., Novelli, A., Fuchs, H., Pullinen, I., Wegener, R.,
669   Rohrer, F., Wildt, J., Scharr, A., Wahner, A., and Mentel, T.: Effects of NO_x and SO_2 on the Secondary Organic
670   Aerosol Formation from Photooxidation of α-Pinene and Limonene, Atmos. Chem. Phys., 18, 1611-1628,
671   https://doi.org/10.5194/acp-18-1611-2018, 2018.

672 Zhou, C., Jang, M., and Yu, Z.: Simulation of SOA Formation from the Photooxidation of Monoalkylbenzenes in
673   the Presence of Aqueous Aerosols Containing Electrolytes under Various NO_x Levels, Atmos. Chem. Phys., 19,
674   5719-5735, https://doi.org/10.5194/acp-19-5719-2019, 2019.